The annual cycle of Northern Hemisphere storm-tracks. Part 1: seasons

Article

Accepted Version

AMERICAN METEOROLOGICAL SOCIETY

Journal of Climate

EARLY ONLINE RELEASE

The DOI for this manuscript is doi: 10.1175/JCLI-D-17-0870.1

The Annual Cycle of Northern Hemisphere Storm-Tracks. Part 1: Seasons

B. J. Hoskins and K. I. Hodges

Department of Meteorology, University of Reading, Reading, United Kingdom.

Corresponding Author: K. I. Hodges
Email: k.i.hodges@reading.ac.uk

Abstract

In this paper and Part 2 a comprehensive picture of the annual cycle of the Northern Hemisphere storm-tracks is presented and discussed for the first time. It is based on both feature tracking and Eulerian based diagnostics, applied to vorticity and meridional wind in the upper and lower troposphere. Here, the storm-tracks, as diagnosed using both variables and both diagnostic techniques, are presented for the four seasons for each of the two levels.

The oceanic storm-tracks retain much of their winter mean intensity in spring with only a small change in their latitude. In the summer they are much weaker, particularly in the Pacific and are generally further poleward. In autumn the intensities are larger again, comparable with those in spring, but the latitude is still nearer to that of summer. However, in the lower troposphere in the eastern ocean basins the tracking metrics show northern and southern tracks that change little with latitude through the year. The Pacific mid-winter minimum is seen in upper troposphere standard deviation diagnostics, but a richer picture is obtained using tracking. In winter there are high intensities over a wide range of latitudes in the central and eastern Pacific, and the west Pacific has high track density but weak intensity. In the lower troposphere all the diagnostics show that the strength of the Pacific and Atlantic storm-tracks are generally quite uniform over the autumn-winter-spring period.

There is a close relationship between the upper tropospheric storm-track, particularly that based on vorticity, and tropopause level winds and temperature gradients. In the lower troposphere, in winter the oceanic storm-tracks are in the region of the strong meridional SST gradients, but in summer they are located in regions of small or even reversed SST gradients. However, over North America the lower tropospheric baroclinicity and the upstream portion of the Atlantic storm-track stay together throughout the year.

1. Introduction

The Northern Hemisphere (NH) winter-time storm-tracks have been the subject of many studies using gridded observational analyses. Sawyer (1970) considered them in terms of daily pressure changes, and Blackmon et al (1977) introduced the use of the variance of the synoptic time-scale band pass filtered fields. A number of studies (e.g. Murray and Simmonds, 1991; Sinclair 1997, Hoskins & Hodges 2002) have returned to the earlier notion of the ensemble of tracks of individual storms. However the NH storm-tracks in other seasons and the annual cycle of the storm-tracks has in general had less attention.

A notable exception to this is the discussion of the mid-winter Pacific storm-track minimum which was first described by Nakamura (1992). He showed that at 250hPa, and using 6-day high-pass filtered height variance, the North Pacific storm-track had a mid-winter minimum between maxima in autumn and spring. He contrasted this with the expected behaviour of a winter maximum in the North Atlantic. In band-pass surface pressure variance he found that the Pacific storm-track amplitude was almost flat over the 5 month period, November to March. The North Pacific mid-winter minimum in the context of the annual cycle has subsequently been discussed by many authors, including Chang (2001), Nakamura and Sampe (2002), Chang and Guo (2007) and Penney et al (2010) (and also very recently Schemm and Schneider, 2018). Spurred on by the discussion of the possible relevance to the Pacific mid-winter minimum of the imprint of eddy feeding from the upstream region, and for its own intrinsic interest, Ren et al. (2010) have considered the annual cycle of storms in a broad East Asian region.

The comparison of the Pacific winter minimum with a more expected winter maximum found in the North Atlantic has often been made, but Ren et al (2014) pointed out that in

71 the NH as a whole, and even to a small extent in the North Atlantic, a mid-winter minimum
72 can be found. Recently, Afargan and Kaspi (2017) have given evidence that an Atlantic
73 winter storm-track minimum is certainly evident in strong jet years.

74 The summer North Atlantic storm-track was the subject of Dong et al (2013), with the
75 emphasis being on its interannual variability. They found a dominant EOF that described a
76 northern or southern storm track location in the 5W-5E sector. They related this mode to
77 the summer North Atlantic Oscillation (NAO) (Folland et al., 2009) and discussed its possible
78 predictability associated with the preceding sea surface temperature anomalies.

79 The studies referred to mostly use a single storm-track diagnostic, which varies between
80 studies, and applied at one, usually upper tropospheric, level. There is mostly a focus on one
81 region of the NH and on the cool season behaviour. Relevant to the annual cycle of the NH
82 storm-tracks an early study of Fleming et al (1987) did discuss the annual cycle of the zonally
83 averaged westerly wind at 500hPa and emphasised the asymmetry of spring and autumn,
84 with the jet some 13° further south in autumn. However, there appears to be no
85 comprehensive study of the full annual cycle of all the NH storm-tracks based on multiple
86 diagnostics applied to the upper and lower troposphere.

87 In this paper the NH storm-tracks for all four seasons will be diagnosed. The metrics used
88 will be based on both band-pass filtered variance and feature tracking diagnostics, applied
89 to both vorticity and meridional wind. The storm-tracks will be diagnosed in both the upper
90 (250hPa) and lower (850hPa) troposphere. One of the points of interest is to compare the
91 nature of the storm-tracks given by the various metrics applied at the two levels. However,
92 the major aim of this paper is to provide new insight into the various NH storm-tracks in the
93 four seasons.

In Part 2 of this paper, a more detailed analysis of the annual cycle of the NH storm-tracks is performed in a number of longitudinal sectors using monthly resolution data.

The organisation of this paper is as follows. The data and methodology used in the study are described in section 2. The diagnostics for the four seasons for the upper tropospheric NH storm-tracks are presented in Section 3, and those for the lower tropospheric storm-tracks in Section 4. Section 5 then gives a discussion of the results.

2. Data and methodology

The main data used in this study is the European Centre for Medium-Range Weather Forecasts (ECMWF) Interim Reanalysis (ERAI) (Dee et al, 2011). This is the most recent reanalysis produced by ECMWF using cycle 31r2 of the Integrated Forecast System (IFS) model and a 4D Variational (4D Var.) data assimilation system with a 12 hour cycle. The forecast model resolution is TL255 (triangular truncation 255, linear grid) spectral resolution in the horizontal and with 60 sigma levels in the vertical. A wide range of observations from terrestrial and space based observing systems are bias corrected (Dee and Uppala, 2009) and assimilated. The data covers the period 1979 till the present. The 6 hourly products are primarily used in this study for the cyclone tracking and band pass filtered diagnostics.

The diagnosis of the seasonal cycle of the NH storm tracks in this study makes use of two methodological approaches, the traditional Eulerian method using the 2-6 day band-pass filtered variance (Blackmon, 1976) and the Lagrangian feature tracking approach. The two approaches have previously been used to provide complementary views of storm track activity in both the Northern (Hoskins and Hodges, 2002; hereafter HH2002) and Southern Hemispheres (Hoskins and Hodges, 2005). The cyclone, feature tracking method used in this study is the same as used in Hoskins and Hodges (2002, 2005) and is based on the feature

117 tracking algorithm of Hodges (1994, 1995, 1999). The algorithm proceeds by spectrally
118 filtering the chosen field to retain synoptic scales in the T6-42 band and additionally applies
119 the tapering filter of Hoskins and Sardeshmukh (1984) to reduce the Gibbs oscillations.
120 Cyclone signatures are then identified as either maxima or minima, depending on the
121 chosen field. This is done on a polar stereographic projection to avoid latitudinal bias in the
122 detection (Hodges, 1995, Sinclair, 1997). Initially the cyclones are identified on the grid on
123 the projection but the locations are then refined using B-spline interpolation and a steepest
124 ascent maximization (Hodges, 1995) which results in smoother tracks. The identified cyclone
125 locations are then converted back to spherical coordinates for the tracking. The tracking
126 proceeds by initially linking points together in consecutive time steps using a nearest
127 neighbour method and the tracks are then refined by minimising a cost function for track
128 smoothness subject to adaptive constraints on displacement distance and track smoothness
129 (Hodges, 1994, 1999). The tracking is performed in spherical coordinates to avoid biases
130 associated with using a projection.

131 Once the tracking is completed, the tracks are filtered to retain the mobile cyclones that
132 last longer than 2 days and travel more than 1000km. The tracks are then used to compute
133 spatial distributions for the track, genesis and lysis densities and for mean properties such as
134 intensity using the spherical kernel method (Hodges, 1996). Here, for space reasons, only
135 track densities and mean intensities will be shown. The track densities will be given in terms
136 of the number per month per unit area that is equivalent to a 5° radius (geodesic) spherical
137 cap, an area of about $(1000\text{km})^2$.

138 For the band-pass filtered variance, the data is first pre-processed in the same way as for
139 the tracking, applying the spatial spectral filtering. The 2-6 day band-pass filtered variance is

obtained using the periodogram method (Kay 1988), based on the Fast Fourier Transform (FFT). Here standard deviations (SD) will be shown.

In HH2002 many fields were used for the investigation of the NH winter storm-tracks, and in particular for cyclone tracking, and the results were compared in some detail. In the IMLAST cyclone track inter-comparison (Neu et al 2013), some used a vorticity-like variable, i.e. geostrophic vorticity computed from the Mean Sea Level Pressure (MSLP) or the lower tropospheric relative vorticity, but MSLP minima were tracked by more than half of the algorithms used, and 850hPa geopotential minima were tracked by others. The advantage of fields such as MSLP and geopotential is that minima in them relate easily to synoptic interpretations of cyclones. However, the major disadvantage is that, as discussed in HH2002, for a feature propagating into a region of ambient low pressure such as the Icelandic Low region, deepening of the centre will occur, but this is not an indication of real development. Further, a changing large-scale background in a changing climate would influence the perceived behaviour of any cyclone feature. Also, the existence of a minimum can be strongly influenced by the ambient pressure gradients (e.g. Sinclair, 1994). Consequently it was seen in HH2002 to be important to remove a background field before tracking, with the tracking results obtained for pressure-like variables being very dependent on whether and how this is done. In addition, as discussed below, mean sea level pressure has the possible disadvantage that in most regions it is an extrapolated field which may be performed differently for different models. For relative vorticity, which in geostrophic terms is proportional to the second derivative of pressure or geopotential, the smaller scales are emphasised. Consequently the results obtained for tracking vorticity maxima are much less dependent on the removal of a smooth background field. There could be a disadvantage that vorticity is an inherently noisier field, and positive vorticity maxima may indicate

different features such as multiple cyclonic centres and various regions along strong fronts. However, this disadvantage can be reduced by using data truncated at less than the full resolution in order to focus on synoptic spatial scales.

In geostrophic terms, the meridional wind involves a single derivative of pressure or geopotential. Therefore, the dependence of the tracking results on the method of removal of the background field is not as large as for geopotential. Further, it does not emphasise the small-scale features as much as vorticity. One significant advantage of considering meridional wind is that it encapsulates the essential ingredient of baroclinic growth: warm air moving poleward (positive V) and ascending east of the cyclone and the cold air moving equatorward (negative V) and descending west of the cyclone (Hoskins and James, 2014).Thus the tracking of meridional wind extrema can be considered to be following the essential elements of synoptic systems. Similarly, band-pass filtered variance of meridional wind is a relevant quantity for depicting storm-tracks that has been used in, for example, Booth et al (2010), HH2002. Chang et al (2002).

For all pressure or height-level measures of the lower tropospheric storm-tracks, extrapolated fields will be used in some regions. For MSLP (and 10m winds which depend on the method of extrapolation and the boundary layer scheme) this problem is most severe. For 850hPa fields there will be regions of significant topography where extrapolated fields are used. However, the storm-tracks are mostly away from such regions, and in any case the modern reanalyses are very careful in their procedures for such extrapolation.

In this paper, in which the focus is on the variation of the storm-tracks over the four seasons, it is not feasible to use the range of storm-track diagnostics evaluated in HH2002. Here, both band-pass variance and feature tracking approaches are applied to 6 hourly

lower (850hPa) and upper tropospheric (250hPa) fields of relative vorticity (ξ) and meridional wind (V). In the NH, vorticity maxima are associated with cyclones and so the tracking is performed on these. In HH2002, the tracking results were shown separately for maxima and minima in V. However, since both northerly and southerly winds are inherent components of a weather system and both are included in variance diagnostics, it is convenient to combine the tracking statistics for the maxima and minima in V. The tracks from both positive and negative V are pooled before computing the spatial statistics which is equivalent to tracking |V| and computing the statistics. The standard deviation of bandpass V can be expected to be almost equally influenced by positive and negative V variations, and so the tracking of $|V|$ is likely to provide the best comparison between the two diagnosis methods. This argument does not apply to vorticity since typical magnitudes of cyclonic relative vorticity extrema dominate over those of anticyclonic extrema.

The focus of this paper and its companion, Part 2, is on describing the annual cycle of the NH storm-tracks and enabling a better understanding of them. For impact studies, the choice of MSLP or near surface winds may be preferable despite the problems discussed above with these variables.

3. Upper Troposphere

In HH2002, the winter season upper tropospheric storm-tracks were analysed using tracking of vorticity maxima at 250hPa (ξ_{250}). In Figure 1 a summary of the results from such an analysis for ξ_{250} maxima is now given for all four seasons; shown in each panel are the track density (contours) and the mean intensity (colour). As seen in HH2002, in winter (Figure 1a) there is a spiral in track density starting near the west coast of North Africa, with successive maxima over the Middle East, the western North Pacific and North America and

continuing over the North Atlantic and Europe and through into northern Asia. The track density maxima are accompanied by high mean intensities. In the central and eastern North Pacific, and to a slightly lesser extent in the North Atlantic, in the winter the high intensities spread to much lower latitudes, though the number of tracks there is relatively small. In summer (Figure 1c) the track density becomes almost a circle at higher latitudes with maxima corresponding to those in winter. The intensity maxima are somewhat smaller than in winter. The spring and autumn pictures are transitional between the two solsticial seasons, but spring (Figure 1b) is generally more similar to winter, and autumn generally more similar to summer in the latitudes of the track density maxima. This is the case in the Atlantic as well as in the Pacific (cf. Lee et al, 2011) and is consistent with the behaviour of the zonally averaged wind found by Fleming et al. (1987). In the two western ocean basins and in all seasons, except for the Pacific in winter, there are clear east-north-east oriented tracks entering from the sub-tropical ocean regions.

From a different perspective, Figure 2 shows the results obtained using the band-pass SD of ξ_{250}. The winter picture (Figure2a) is dominated by a single region of high values extending from the central Pacific, across North America to a maximum in the Atlantic. From here there are weaker extensions into northern Eurasia and the Middle East, the former linking across Siberia to the entrance of the Pacific storm-track. It is interesting to compare this with the tracking picture (Figure 1a). In SD, the single storm-track in winter shows indications of separation into Pacific and Atlantic tracks in the other seasons, whereas in track density the separation into an Eurasian-Pacific track and a North American-Atlantic track is marked in all seasons. For winter in the western Pacific, the maximum SD values are relatively low, reflecting the relatively low mean intensities in the narrow region of high track density there. The link from northern Eurasia and across Siberia seen in the SD is

235 associated with track density more than intensity. The North African and Middle East high
236 track density and high intensity is apparent in SD as the lower latitude extension of the
237 Atlantic maximum, though it is not as prominent. In spring (Figure 2b) and autumn (Figure
238 2d) there is a marked Pacific maximum in SD and there is more linkage across northern
239 Eurasia, so that the patterns appear more circular than in winter. Summer (Figure 2c) shows
240 much weaker maxima than the other seasons, particularly in the Pacific, and these occur in
241 a higher latitude ring that is consistent with the track density and mean intensity pictures
242 (Figure 1c). The autumn oceanic storm-tracks are again seen to be poleward of those in
243 spring.

244 The results for tracking 250hPa meridional wind are shown in Figures 3 and 4. Figure 3
245 gives the track density and intensity separately for positive and negative V extrema in DJF,
246 and Figure 4 the same statistics for |V| for the four seasons. Therefore the two panels of
247 Figure 3 can be compared with Figure 4a to see the relative contributions of positive and
248 negative extrema in winter to the |V| results. It is apparent that positive *V* generally makes
249 the major contribution to the track density. The major exception is the negative *V* track
250 density maximum in Siberia, presumably related to cold air outbreaks there, as discussed by
251 for example Joung and Hitchman (1982). Elsewhere, negative *V* gives high intensity in the
252 lower latitude Central Pacific, across N America and on the downstream side of the N
253 Atlantic storm-track, to the south of the UK. In the three other seasons (shown in
254 Supplementary Material) the contributions of the positive and negative *V* to |*V*| track
255 density are more comparable in magnitude. In all four seasons, the negative extrema are
256 important in their intensity from the Central Pacific to North America and south of the UK.
257 Its Siberian track density maximum is also marked except in JJA.

Turning to the combined statistics for $|V_{250}|$ in Figure 4 and comparing with the results for vorticity, the winter track density for $|V_{250}|$ (Figure 4a) is more dominated by the structure at higher latitudes than is the case for tracking ξ_{250} (Figure1a) and hence appears more circular. However, the high intensities are mostly in the region from the central Pacific through to Western Europe. The occurrence of a small number of systems with high intensity at lower latitudes, mostly from negative V events, is again seen in the Pacific, and to a lesser extent in the Atlantic. High track density is here seen to occur in a band from northern Eurasia to the west Pacific, but with generally small intensities. The subtropical track seen in the ξ_{250} tracking is evident here also in the track density extension over the Middle East, but is associated with relatively weak intensity values. Because vorticity emphasises smaller scales than meridional wind, the smaller amplitude of the subtropical tracks using V implies that these are regions of generally smaller scale systems compared with the higher latitudes.

In contrast to winter, spring (Figure 4b) shows a track density that is largest in the western and central Pacific. However, in summer (Figure 4c) smaller track densities and intensities are found there. The oceanic tracks are generally shifted poleward in summer and the track densities in the western Atlantic are actually largest then, though the intensities are reduced compared with the other seasons. The autumn track density (Figure 4d) is quite similar in latitude and amplitude to that in summer but the intensities are comparable with those in spring and winter.

The seasonal results for the band pass SD of V_{250} (Figure 5) are quite similar in all seasons to those for the same diagnostic applied to ξ_{250} (Figure 2). The proportional reduction from winter to summer is greater, particularly in the North Pacific, consistent with the notion that

281 the scale of systems is smaller in summer, particularly in the North Pacific. Comparing with
282 the tracking of $|V_{250}|$ (Figure 3), there is considerable similarity, though it is apparent that
283 the SD generally reflects the mean intensities rather more than the track densities. For
284 example, the winter Pacific maximum in SD is influenced by the relatively small number of
285 lower latitude high intensity systems. The northern Eurasian track density maximum in
286 summer is a weak feature in SD, consistent with the low mean intensities there.

287 The differing perspectives on storm-tracks given by the various metrics can be illustrated
288 by comparison between them in terms of the relative intensities of the northern and
289 southern storm-track branches over eastern Asia in winter. Vorticity tracking (Figure 2a)
290 emphasises the southern branch, whereas vorticity and meridional wind SD and meridional
291 wind tracking all emphasise the northern branch. This is consistent with the southern
292 branch containing coherent small-scale wave-like structures in vorticity. As discussed
293 above, the northern branch is dominated by tracks of extrema in northerly winds.

294 To link with theoretical ideas it is useful to compare the 250hPa storm-track results with
295 relevant mean state fields in the upper troposphere. The left hand panels of Figure 6 show
296 for winter (Figure 6a) and summer (Figure 6c) two such fields on the dynamic tropopause
297 defined as the PV=2 surface (Hoskins et al., 1985; Hoskins and James 2014): the zonal wind,
298 U (contours), and the negative of the meridional potential temperature gradient, $-\theta_y$ (
299 colours). Using the PV2 surface for U has the theoretical advantage that it shows both the
300 subtropical and midlatitude jets at their tropopause-level maxima. However, U on 250hPa
301 (not shown) is actually very similar to that on PV2. The $-\theta_y$ calculated on the PV2 surface
302 indicates the mean state tropopause gradients that are relevant for both Rossby wave
303 propagation and baroclinic instability (Hoskins and James, 2014). In general the maxima of

304 the two fields are closely aligned, though the winter extension of the North Atlantic jet
305 towards North-West Europe is less marked in $-\theta_y$ than the linkage with the entrance to the
306 sub-tropical jet over North Africa.

307 All the storm-track measures given in Figures 1-3 and 5 show a strong relationship with
308 the mean fields given in Figure 6. However, the correspondence is particularly striking for
309 the positive vorticity tracking measures (Figure 1 a, c). To illustrate this, Figure 6 (b) and (d)
310 have contours of $-\theta_y$ (colours) as in Figs 5 (a) and (c), respectively, overlaid with contours of
311 positive ξ_{250} track density. Strong positive vorticity features are consistently found to occur
312 slightly poleward of the U and $-\theta_y$ maxima. This is the case even for the east-north-east
313 oriented tracks in the sub-tropical ocean regions in the two western ocean basins, which are
314 present in all seasons apart from the Pacific in winter. In summer these regions are on the
315 eastern edge of the two mid-oceanic troughs. The intimate relationship between the upper
316 tropospheric storm-tracks and the maxima in U and $-\theta_y$ is consistent with the notion that
317 vorticity features in the upper troposphere have a predominantly local Rossby wave-like
318 nature. However, the track densities for V_{250} in, for example in the North Atlantic, extend
319 eastwards in middle latitudes beyond regions of maximum $-\theta_y$. This is suggestive that the
320 development downstream is associated with advection and with coupling with lower layers
321 of the atmosphere as in baroclinic instability. Since vorticity emphasises smaller horizontal
322 scales, and the vertical scale of features can be expected to scale as f/N times the horizontal
323 scale (Hoskins and James, 2014), vorticity features are more likely to be shallower and to
324 exist as waves on the upper tropospheric PV gradients. This may correspond to the trapping
325 in the upper troposphere discussed by Nakamura and Sampe (2002). Meridional wind
326 features can be expected to be deeper and more likely to lead to development through
327 interaction with mid-latitude near-surface temperature gradients.

4. Lower troposphere

In this section, the storm-track diagnostics used in Section 3 for the upper troposphere will now be applied to variables at the 850hPa level. Tracking of positive vorticity features at 850hPa (ξ_{850}, Figure 7) picks out the separate Pacific and Atlantic storm-tracks in all seasons. In both cases, the track densities have a slight maximum in winter, and the intensities have a strong minimum in summer. As in the upper troposphere, the storm-tracks are generally further poleward in summer than winter, and the autumn storm-track latitudes are more similar to those of summer and spring latitudes more similar to those of winter. However, the eastern sides of the two ocean basins show a different behaviour. In the eastern Pacific there are two maxima in track density that have similar locations throughout the year, with the northern one dominating in track density and mean intensity in summer and autumn. In the eastern Atlantic, the bias of the track to the north and through Iceland is actually less dominant in summer. The two tracks over eastern Asia feeding into the Pacific storm-track are particularly noticeable in spring (Figure 7b). The northern track is equally marked in autumn (Figure 7d), and slightly less in winter, but the southern one is less clear in these seasons. Both are weak in the summer.

In contrast with the same field in the upper troposphere (Figure 1), the Atlantic and Pacific storm-tracks have track density and intensity well aligned in the two major oceanic storm-tracks and there is in general little indication of activity in the sub-tropical jet region. The major exceptions to this are the southern China track in spring and the Mediterranean track in winter and spring. However, even in these seasons and regions, the intensities are relatively weak. There are signs of a split in the Mediterranean track density in spring with a secondary region being present over North Africa. The spring cyclones in this region have been studied by, for example, Alpert and Ziv (1989).

The band-pass SD of ξ_{850} generally gives seasonal pictures (Figure 8) that are very similar to those that are given by tracking (Figure 7), which is consistent with the alignment of track density and intensity commented on above. The Pacific storm-track shows similar values in winter and spring, and is slightly weaker in autumn but considerably weaker in summer. In contrast, in this measure the Atlantic storm-track is definitely strongest in winter. However, the intensity there in summer is not as weak as in the Pacific. The western and central portions of the Pacific storm-track and the western portion of the Atlantic storm-track are shifted poleward in summer and autumn. In the eastern ocean basins the behaviour is not as clear as in the tracking picture. However, again the lack of simple poleward movement in summer is apparent. The well separated Pacific and Atlantic storm-tracks in the lower troposphere contrast with the upper tropospheric single storm-track behaviour found with this diagnostic (Figure 2). The Mediterranean storm-track is again clearly delineated in winter and spring. Though not the subject of this paper, the signatures of West African and East Pacific Easterly Waves and the typhoon related maximum north-east of the Philippines are all seen in summer near the boundaries of the plots.

As for the upper troposphere, tracking results for *V* at 850hPa are shown in Figure 9 separately for positive and negative V extrema in DJF, and in Figure 10 for $|V_{850}|$ for the four seasons. The two panels of Figure 9 can be compared with Figure 10a to see the contributions of the positive and negative V_{850} extrema in winter. The track densities and intensities for positive and negative *V* are broadly similar but are generally slightly smaller for negative *V*. For the Atlantic track, negative V is important near the coast of N America, but positive V is dominant over the mid-ocean. The former is consistent with cold outbreaks from the continent and the latter with the south-west to north-east tilt of the storm-track. On the eastern side of each ocean basin, negative V has a track at lower latitudes and

376 positive V at higher latitudes. These clearly correspond to the southern and northern tracks,
377 respectively, in the vorticity tracking (Figure 7). In the Mediterranean, negative V is
378 dominant in the west and positive V in the east, consistent with cold and warm outbreaks,
379 respectively, in the two regions. In the northern East Asian, Siberian, track negative V is
380 dominant. As in the upper troposphere, this is consistent with the cold out-breaks there.
381 These comments apply also in other seasons (See Figure S2 in Supplementary Material),
382 except that the negative V extrema are found in the Mediterranean only in winter and
383 spring.

384 In contrast to the upper troposphere, at 850hPa the tracking of |V| maxima (Figure 10)
385 gives generally very similar results to those for tracking positive vorticity (Figure 6). There is
386 a clear indication of a winter maximum in the occurrence of |V| extrema in the lee of the
387 Rockies, consistent with Hsu (1987). There is also more evidence in all seasons of a north
388 Russian storm-track, with some linkage to the Atlantic storm-track and perhaps also linking
389 up with the Siberian feed into the Pacific storm-track. The Mediterranean track is again
390 marked in winter and spring, with a slight southward shift in the latter. This may be
391 compared with the appearance of a secondary track over North Africa seen in vorticity
392 tracking (Figure 10c compared with Figure 7c). This suggests that the systems over North
393 Africa generally have a smaller scale and are therefore more marked in vorticity. The
394 easterly wave and tropical cyclone signatures are all apparent in summer as they were when
395 tracking positive vorticity.

396 The band-pass SD of V_{850} (Figure 11) gives a picture that is consistent with, but less
397 detailed than, that obtained with tracking. The decrease in amplitude from winter to

summer is particularly apparent. The spring Mediterranean maximum is here marked and centred over the coast of North Africa.

Briefly we now consider storms in two regions that are not the major focus of this paper. In both Figures 7 and 10, the tracks of African Easterly waves (Thorncroft and Hodges, 2001), moving westwards into the Atlantic from West Africa are evident in summer and to a lesser extent in autumn. Similar signatures are seen in the East Pacific in summer and autumn for tropical cyclones there. In both seasons, the track densities indicate the westward movement of tropical cyclones into the West Pacific. Those that intensify into typhoons and recurve towards the north (see e.g. Harr and Elsberry, 1995) lead to the intensity maxima north-east of the Philippines, these being particularly striking in autumn. However no such signatures are apparent in the tropical West Atlantic where tropical cyclone numbers are generally lower.

The annual cycle of storms in the Arctic is also apparent in the Figures presented here. Tracking (Figures 7 and 10) shows winter-time tracks from the north-east Atlantic and significant intensity over much of the Arctic (apart from Greenland where the data at this level is artificial). In summer there are smaller intensities but there is a track north of Siberia. These aspects are consistent with Serreze et al (1993) and Serreze and Barrett (2008), and the influence in summer of land-sea temperature contrasts as discussed by Day and Hodges (2017).

Returning attention to the two major lower tropospheric oceanic storm-tracks, to examine their relationship with seasonal mean temperature gradients, Figure 12 shows winter (upper row) and summer (lower row) contours of the SD of V_{850} overlaid on meridional gradients of sea surface temperature (SST, left) and 850hPa temperature (T_{850},

421 right). It should be noted that in regions of significant topography, surface pressure would
422 be less than 850 hPa and the values there are extrapolations. The signs of the gradients are
423 reversed so that red contours correspond to temperatures decreasing towards the pole. In
424 winter (Figure 10a), the Pacific storm-track is generally at the latitude of the maximum SST
425 gradients and downstream from the largest values. In the Atlantic, the region of the highest
426 variance contour coincides with much of the strong Gulf Stream SST gradient, though also
427 with a little of the reversed gradient, particularly on the poleward flank. However in summer
428 (Figure 10c), both storm-tracks have moved poleward of the maximum SST gradients that
429 can be expected to aid growth and include regions of reversed SST gradient. The T_{850}
430 gradient fields (Figure 12b, d) are generally a slightly smoother version of the SST gradients
431 over both ocean basins and in both seasons. However, over North America, the upstream
432 portion of the Atlantic storm-track and the region of largest temperature gradients are
433 generally coincident and move poleward together. In winter there are marked T_{850} gradients
434 over eastern Asia upstream of the two feeding regions for the Pacific storm-track.

435

436 ## 5. Discussion

437 For the first time, a comprehensive view of the upper and lower tropospheric NH storm-
438 tracks in all four seasons has been presented. This has been done using four sets of storm-
439 track metrics, standard deviation (SD) of both band-pass vorticity and meridional wind, and
440 tracking (showing track density and mean intensity) of both positive vorticity maxima and
441 meridional wind extrema. There is a general similarity between the four sets of diagnostics,
442 but there are many difference in detail that give insights into differences in the nature of the
443 storm-track through the year, and from one region to another. Smaller scale systems are

444 emphasised more by vorticity than by meridional wind. High SD values can be related to
445 high mean intensity or high track density, but more usually the former. High SD values in the
446 absence of high track density or intensity is an indication of many systems without
447 systematic movement over a 2 day period. The opposite may indicate that systems are small
448 and fast moving and not well captured by the 2-day lower limit of the band-pass filter or
449 that they have power at periods longer than 6 days.

450 The main focus of this paper is the differing structures of the storm-tracks in the four
451 seasons. The general behaviour is that the storm-tracks in both the upper and lower
452 troposphere retain much of their winter mean intensity in spring and there is only a small
453 change in their latitude. The summer storm-tracks are weaker and generally further
454 poleward. In autumn the intensities are larger again, comparable with those in spring, but
455 the latitude is still nearer to that of summer. The positive difference in the latitudes of the
456 autumn and spring storm-tracks is consistent with the behaviour of the zonally averaged
457 westerly winds found by Fleming et al (1987) and is an example of inertia in the climate
458 system, and is consistent with the large heat capacity of the ocean.

459 As seen in all the metrics, the poleward shift of the lower tropospheric oceanic storm-
460 tracks in summer and autumn does not occur in the eastern ocean basins. Tracking of
461 vorticity and |V| shows there to be two tracks into western N America and Europe that shift
462 little with season. Separate tracks of positive and negative near the boundaries of the plots
463 show that the northern track is dominated by maxima in southerly winds and the southern
464 tracks by maxima in northerly winds.

465 The mid-winter minimum in the Pacific storm-track is apparent in the upper tropospheric
466 SD results based on both vorticity and meridional wind (Figures 2a and 4a). This is consistent

467 with Nakamura (1992) in which geopotential was used. The tracking diagnostics (Figure 1a
468 and 3a) show that in winter there is less coherence to the storm-track than in the other
469 seasons. The region of large intensities broadens and spreads to the low latitude oceanic
470 regions. SD values are indeed reduced in winter in the storm-track but there are more
471 strong systems over the lower latitude Pacific Ocean. Separate tracking of positive and
472 negative V shows that there are strong northerlies associated with these systems. In the
473 lower troposphere all the diagnostics show that the strength of the Pacific storm-track is
474 quite flat over the autumn-winter-spring period. This is consistent with Nakamura (1992)
475 who found that there was little change in the variance of band-pass mean sea level pressure
476 from November to March. Similar results are found in the Atlantic, though, depending on
477 the metric used, there can be a weak winter maximum in the storm-track.

478 The relative weakness of the summer storm-tracks compared with those in winter, as
479 measured by SD, is more apparent in meridional wind than vorticity, consistent with the
480 smaller scales of summer systems. The reduction in the Pacific is larger than in the Atlantic,
481 but this may be partially associated with the longer periods of some Pacific systems in
482 summer, as found by Chang (1999), with some power occurring outside the traditional 2-6
483 day band-pass filter used in the SD analysis. This was also highlighted by Burkhardt and James
484 (2006) who suggested care is required in interpreting band pass filtered eddy variances in the
485 presence of large changes in jet intensity. In the lower troposphere in the Atlantic, the track
486 densities in summer are actually comparable to those in winter. It is the mean intensities
487 that are much reduced.

488 In tracking, the general dominance, particularly in the lower troposphere, of positive V
489 over negative V in their contribution to extrema in |V| may be associated with the fact that

latent heat release occurs in the ascending, poleward moving air leading to intensification of this branch.

Indications of a northern Russian storm-track are seen in both the upper and lower troposphere in many fields and most seasons, somewhat separated from but a possible extension of the N Atlantic track. This is associated mostly with maxima in southerly winds. To the east, over Siberia, and again possibly linked, there is a strong maximum in track density at both levels in all seasons except summer, but this is associated with maxima in the northerlies, presumably associated with cold air out-breaks.

On the strong subtropical jet across Eurasia, there is a narrow but strong track in upper tropospheric vorticity. This is less marked in other measures. However, the SD of *V* and vorticity do indicate an eastwards extension around 30°N of the Mediterranean/Middle East track to near 110°E, and a smaller extension is also seen in the tracking of *V*. This is suggestive that vorticity tracking is predominantly picking up shallow small-scale features moving rapidly along the jet. In the other fields, the extension across southern Asia near 30°N may be related to the southern Asia track highlighted by Chang (2005) as being linked to subsequent surface cyclogenesis over the N Pacific. Consistent with this interpretation, the average phase speed in this region for tracked vorticity features is about 20ms^{-1}, whereas for tracked *V* features it is about 16ms^{-1}. This is still larger than the 10ms^{-1} or less found by Chang and Yu (1999), but it is possible that it is the slower features in this region that are more likely to be linked to later surface cyclogenesis. In addition, the 8-10 day period found by Chang and Yu (1999) means that the signature of these slow features may be underestimated in an SD analysis based a on a 2-6 day band-pass filter.

513 The lower tropospheric Mediterranean storm-track is marked in winter and spring, with
514 evidence of increased North African activity in spring given by a secondary track in vorticity
515 and a southward shift of the main track in meridional wind. The cyclones occurring on the
516 spring-time enhanced baroclinicity in this region have been discussed by Alpert and Ziv
517 (1989). In the western Mediterranean the northerly extrema are generally dominant,
518 consistent with the cold outbreaks there. However, southerly extrema tend to dominate in
519 the eastern basin.

520 It has been shown that the relationship of the upper and lower storm-tracks to relevant
521 mean state variables is mostly a close one. In the upper troposphere (Figure 6) the winter
522 and summer storm-track, particularly as diagnosed by vorticity tracking, predominantly lie
523 just poleward of the tropopause westerly wind and equatorward potential temperature
524 gradient maxima. In the lower troposphere, in winter, the oceanic storm-tracks are in the
525 region of the strong meridional SST gradients (Figure 10). However, the more poleward
526 summer storm-tracks have their maxima in regions of small or even reversed SST gradient.
527 In contrast, the upstream portion of the Atlantic storm-track and the lower tropospheric
528 baroclinicity over North America remain coincident throughout the year, moving together in
529 latitude. This is consistent with the smaller decrease in intensity of the Atlantic storm-track
530 in summer compared with that in the Pacific.

531 The diagnostics exhibited in this paper contain many interesting features, and it has been
532 possible here to produce only an overview. In Part 2 of this paper the annual cycle of the
533 storm-tracks is examined in more detail in particular longitudinal sectors using monthly
534 resolution.

535

Acknowledgements

We thank Tim Woollings for provoking us into extending our previous analysis of NH storm-tracks into other seasons, and Paul Berrisford and the ECMWF Reanalysis team for the provision of the basic data used in this paper. We also thank the reviewers, whose critical comments have led to many improvements in this paper.

References

Afargan, H. and Y. Kaspi, 2017: A midwinter minimum in North Atlantic storm track intensity in years of a strong jet. *Geophys. Res. Lett.*, doi: 10.1002/2017GL075136

Alpert, P., and B. Ziv, 1989: The Sharav Cyclone: Observations and some theoretical considerations, *J. Geophys. Res.*, **94**, 18495–18514.

Booth, J., L. Thompson, J. Patoux, K. A. Kelly and S. Dickinson, 2010: The Signature of the Midlatitude Tropospheric Storm Tracks in the Surface Winds. *J. of Climate*. **23**, 10.1175/2009JCLI3064.1.

Blackmon, M. L., J. M. Wallace, N.-C. Lau, and S. L. Mullen, 1977: An observational study of the Northern Hemisphere wintertime circulation. *J. Atmos. Sci*., **34**, 1040–1053.

Chang, E.K.M., and D.B. Yu, 1999: Characteristics of wave packets in the upper troposphere. Part I: Northern hemisphere winter. J. Atmos. Sci., 56, 1708-1728.

Burkhardt, Ulrike & N. James, Ian. (2006). The effect of Doppler correction on measures of storm track intensity. Climate Dynamics. 27. 515-530. 10.1007/s00382-006-0146-4.

Chang, E.K.M., 1999: Characteristics of wave packets in the upper troposphere. Part II: Hemispheric and seasonal differences. J. Atmos. Sci., 56, 1729-1747.

Chang, E. K. M., 2001: GCM and observational diagnoses of the seasonal and interannual variations of the Pacific storm track during the cool season., *J. Atmos. Sci.*, **58**, 1784–1800.

Chang, E. K. M., S. Lee and K. L. Swanson, 2002: Storm track dynamics, *J. of Clim*. **15** 2163–2183.

Chang, E.K.M., 2005: The impact of wave packets propagating across Asia on Pacific cyclone development. Mon. Wea. Rev., 133, 1998-2015.

564 Chang, E. K. M., and Y. Guo, 2007: Dynamics of the stationary anomalies associated with the
565 interannual variability of the midwinter Pacific storm track—The roles of tropical heating
566 and remote eddy forcing. *J. Atmos. Sci.*, **64**, 2442–2461.
567 Day, J. J., and K. I. Hodges, 2017: The influence of Arctic land-sea temperature contrasts on
568 northern hemisphere summer circulation. *Nat. Geo.*, submitted.
569 Dee, D. P., and Co-authors, 2011: The ERA-Interim reanalysis: Configuration and
570 performance of the data assimilation system. *Q. J. Roy. Meteor. Soc*. **, 137** , 553–597, doi:
571 10.1002/qj.828.
572 Dee, D. P., and S. M. Uppala, 2009: Variational bias correction of satellite radiance data in
573 the ERA-Interim reanalysis. *Q. J. Roy. Meteor. Soc*., **135**, 1830–1841, doi:10.1002/qj.493
574 Dong, B., R. T. Sutton, T. Woollings, and K. Hodges, 2013: Variability of the North Atlantic
575 summer storm track: mechanisms and impacts on European climate, *Environ. Res. Lett.,* **8**,
576 doi: 10.1088/1748-9326/8/3/034037.
577 Fleming, E. L., H. G.-Lim, and J. M. Wallace, 1987: Differences between the spring and
578 autumn circulation of the Northern Hemisphere, *J. Atmos.Sci.,* **44**, 1266–1286.
579 Folland, C.K., J. Knight, H. W. Linderholm, D. Fereday, S. Ineson, and J. W. Hurrell, 2009: The
580 summer North Atlantic Oscillation: past, present, and future. *J. Clim.* **22**, 1082–1103.
581 Harr, P. A., and R. L. Elsberry, 1995: Large-scale circulation variability over the tropical
582 western North Pacific. Part I: Spatial patterns and tropical cyclone characteristics. *Mon.*
583 *Wea. Rev.*, **123**, 1225–1246.
584 Hodges, K. I., 1994: A general method for tracking analysis and its application to
585 meteorological data.
586 *Mon. Wea. Rev*., **122**, 2573–2586.
587 Hodges, K. I., 1995: Feature tracking on the unit sphere. *Mon. Wea. Rev*., **123**, 3458–3465.

588 Hodges, K. I., 1996: Spherical nonparametric estimators applied to the UGAMP model
589 integration for AMIP, *Mon. Wea. Rev.,* **124**, 2914–2932.
590 Hodges, K. I., 1999: Adaptive constraints for feature tracking. *Mon. Wea. Rev*., **127**, 1362–
591 1373.
592 Hoskins, B. J. and K. I. Hodges, 2002: New perspectives on the Northern Hemisphere winter
593 storm tracks. *J. Atmos. Sci.,* **59**, 1041–1061.
594 Hoskins, B. J. and K. I. Hodges, 2005: New perspectives on the Southern Hemisphere storm
595 tracks. *J. Clim.*, **18**, 4108–4129.
596 Hoskins, B. J. and I.N. James, 2014: Theme 2: Rotation in the atmosphere, in Fluid Dynamics
597 of the Midlatitude Atmosphere, John Wiley & Sons, Ltd, Chichester.
598 doi: 10.1002/9781118526002.ch8
599 Hoskins, B. J., M. E. McIntyre, and A. W. Robertson, 1985: On the use and significance of
600 isentropic potential vorticity maps, *Q. J. R. Meteorol. Soc*., **111**, 877–946.
601 Hoskins, B. J., and P. D. Sardeshmukh, 1984: Spectral smoothing on the sphere. *Mon. Wea.*
602 *Rev*., **112**,
603 2524–2529.
604 Hsu, H-H., 1987: Propagation of low-level circulation features in the vicinity of mountain
605 ranges. *Mon. Wea. Rev.*, **115,** 1864–1892.
606 Kay, S. M., 1988: Modern Spectral Estimation—Theory and Application. Prentice-Hall, 543
607 pp.
608 Joung, C. H. and M. H. Hitchman, 1982: On the role of successive downstream development in
609 East Asian polar air outbreaks. *Mon. Wea. Rev.*, **110**, 1224–1237.

610 Lee, S. S., J. Y. Lee, B. Wang, F.-F. Jin, W.-J. Lee and K.-J. Ha, 2011: A comparison of
611 climatological subseasonal variations in the wintertime storm track activity between the
612 North Pacific and Atlantic: local energetics and moisture effect*, Clim. Dyn.,* **37,** 2455.
613 https://doi.org/10.1007/s00382-011-1027-z.
614 Murray, R. J., and I. Simmonds, 1991: A numerical scheme for tracking cyclone centres from
615 digital data. Part I: Development and operation of the scheme, *Aust. Meteor. Mag.,* **39**, 155–
616 166.
617 Nakamura, H., 1992: Midwinter suppression of baroclinic wave activity in the Pacific. *J.*
618 *Atmos. Sci.,*
619 **49**, 1629–1642.
620 Nakamura, H., and T. Sampe, 2002: Trapping of synoptic-scale disturbances into the
621 North-Pacific subtropical jet core in midwinter. *Geophys. Res. Lett.*, **29**,
622 doi:1029/2002GL015335 .
623 Penny, S., G. Roe, and D. Battisti, 2010: The source of the midwinter suppression in
624 storminess over the North Pacific, *J. Climate*, **23** , 634–648.
625 Ren, H.-L., F.-F. Jin, and J.-S. Kug, 2014: Eddy-induced growth rate of low-frequency
626 variability and its mid-to late winter suppression in the Northern Hemisphere. *J. Atmos.*
627 *Sci.*, *71* (7), 2281–2298.
628 Ren, X., X. Yang, and C. Chu, 2010: Seasonal variations of the synoptic-scale transient
629 eddy activity and polar front jet over east Asia. *J. Climate*, **23** , 3222–3233.
630 Sawyer, J. S., 1970: Observational characteristics of atmospheric fluctuations with a time
631 scale of a month. *Q. J. R. Meteorol. Soc*., **96**, 610–625.

632 Schemm, S., and T. Schneider, 2018: **Eddy lifetime, number, and diffusivity and the suppression of**
633 **eddy kinetic energy in midwinter**. *Journal of Climate*, **31**, 5649-5665.

634 Serreze, M. C., J. E. Box, R. G. Barry and J. E. Walsh, 1993: Characteristics of Arctic synoptic
635 activity. *Meteor. Atmos. Phys*., **51**, 147-164.

636 Serreze, M. C. and A. P. Barrett, 2008: The summer cyclone maximum over the Central
637 Arctic Ocean, *J. Clim.*, **21**, 1048–1065.

638 Sinclair, M. R., 1994: An objective cyclone climatology for the Southern Hemisphere. *Mon.*
639 *Wea. Rev.,* **122,** 2239–2256.

640 Sinclair, M. R., 1997: Objective identification of cyclones and their circulation intensity and
641 climatology. *Wea. Forecasting*, **12**, 595–612.

642 Thorncroft, C. D., and K. Hodges, 2001: African easterly wave variability and its relationship
643 to Atlantic tropical cyclone activity. *J. Clim.*, **14**, 1166–1179.

644

Captions

Figure 1 Track density (contours) and mean intensity (colour) of 250 hPa vorticity (ξ_{250}) maxima for each season, (a) DJF, (b) MAM, (c) JJA and (d) SON. Track density contours are every 2.5 with the dashed line at 12.5 in units of number per month per unit area, where the unit area is equivalent to a 5^0 spherical cap. The intensity is in units of 10^{-5} s^{-1}. Mean intensity is suppressed for track densities below 1.0.

Figure 2 Standard deviation of 2-6 day band pass filtered variance of ξ_{250} for (a) DJF, (b) MAM, (c) JJA and (d) SON. Units are 10^{-5} s^{-1}.

Figure 3 Track density (contours) and mean intensity (colour) for (a) positive anomalies and (b) negative anomalies in the 250hPa meridional wind (V_{250}) for DJF. Track density contours are every 2.5 with the dashed line at 10.0 in units of number per month per unit area, where the unit area is equivalent to a 5^0 spherical cap. The intensity is in units of m s^{-1}. Mean intensity is suppressed for track densities below 1.0.

Figure 4 Track density (contours) and mean intensity (colour) for extrema in the 250hPa meridional wind (V_{250}) for each season, (a) DJF, (b) MAM, (c) JJA and (d) SON. Track density contours are every 2.5 with the dashed line at 12.5 in units of number per month per unit area, where the unit area is equivalent to a 5^0 spherical cap. The intensity is in units of m s^{-1}. Mean intensity is suppressed for track densities below 1.0.

Figure 5 Standard deviation of 2-6 day band pass filtered variance of V_{250} for (a) DJF, (b) MAM, (c) JJA and (d) SON. Units are m s^{-1}.Figure 6 Tropopause level (PV=2) mean fields and the 250hPa storm-track are shown for winter (upper panels: a, b) and summer (lower panels: c, d). In each panel the mean meridional gradient of $\theta_{PV=2}$ is shown in colour with

667 reversed sign and in units of K (100km)$^{-1}$. In the panels on the left (a, c), the overlaid field is
668 the seasonal mean zonal wind, $U_{PV=2}$, with contours every 10ms^{-1} and negative values in
669 white with dashed contour at ±30ms^{-1}. In the panels on the right (b, d), the overlaid field is
670 the track density for ξ_{250} cyclones, as in Fig.1.

671 Figure 7 Track density (contours) and mean intensity (colour) of ξ_{850} cyclones for each
672 season, (a) DJF, (b) MAM, (c) JJA and (d) SON. Track density contours are every 2.5 with the
673 dashed line at 12.5 in units of number per month per unit area, where the unit area is
674 equivalent to a 5^0 spherical cap. The intensity is in units of 10^{-5} s^{-1}. Mean intensity is
675 suppressed for track densities below 1.0.

676 Figure 8 Standard deviation of 2-6 day band pass filtered variance of ξ_{850} for (a) DJF, (b)
677 MAM, (c) JJA and (d) SON. Units are 10^{-5} s^{-1}.

678 Figure 9 Track density (contours) and mean intensity (colour) for (a) positive anomalies and (b)
679 negative anomalies in the 850hPa meridional wind (V850) for DJF. Track density contours are
680 every 2.0 with the dashed line at 8.0 in units of number per month per unit area, where the
681 unit area is equivalent to a 50 spherical cap. The intensity is in units of m s-1. Mean intensity
682 is suppressed for track densities below 1.0.

683 Figure 10 Track density (contours) and mean intensity (colour) for extrema in V_{850} for each
684 season, (a) DJF, (b) MAM, (c) JJA and (d) SON. Track density contours are every 2.5 with the
685 dashed line at 12.5 in units of number per month per unit area, where the unit area is
686 equivalent to a 5^0 spherical cap. The intensity is in units of m s^{-1}. Mean intensity is
687 suppressed for track densities below 1.0.

688 Figure 11 Standard deviation of 2-6 day band pass filtered variance of V_{850} for (a) DJF, (b)
689 MAM, (c) JJA and (d) SON. Units are m s^{-1}.

690 Figure 12 Low-level mean temperature gradients and the 850hPa storm-track are shown for
691 winter (upper panels: a, b) and summer (lower panels: c, d). The contours in each panel are
692 those of the standard deviation of 2-6 day band-pass filtered variance of V_{850} for the
693 relevant season with contours every 1 ms^{-1} and the 5ms^{-1} contour dashed. Colour contours
694 are for the mean meridional gradient of sea surface temperature (left: a, c) and 850hPa
695 temperature (right: b, d). In each case, the sign has been reversed and the unit is K $(100Km)^{-1}$.
696

Figures

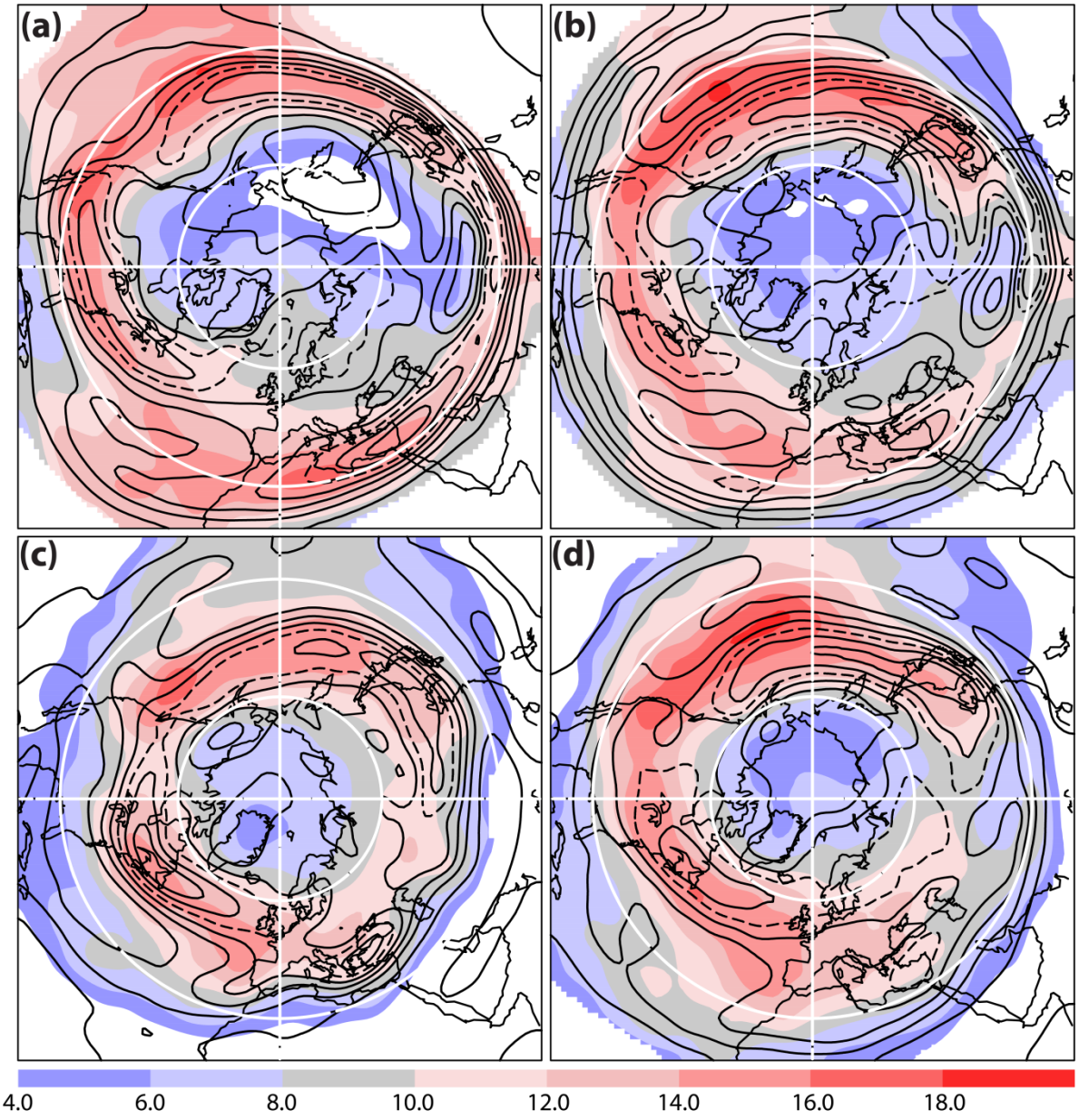

Figure 1 Track density (contours) and mean intensity (colour) of 250 hPa vorticity (ξ_{250}) maxima for each season, (a) DJF, (b) MAM, (c) JJA and (d) SON. Track density contours are every 2.5 with the dashed line at 12.5 in units of number per month per unit area, where the unit area is equivalent to a 5^0 spherical cap. The intensity is in units of 10^{-5} s^{-1}. Mean intensity is suppressed for track densities below 1.0.

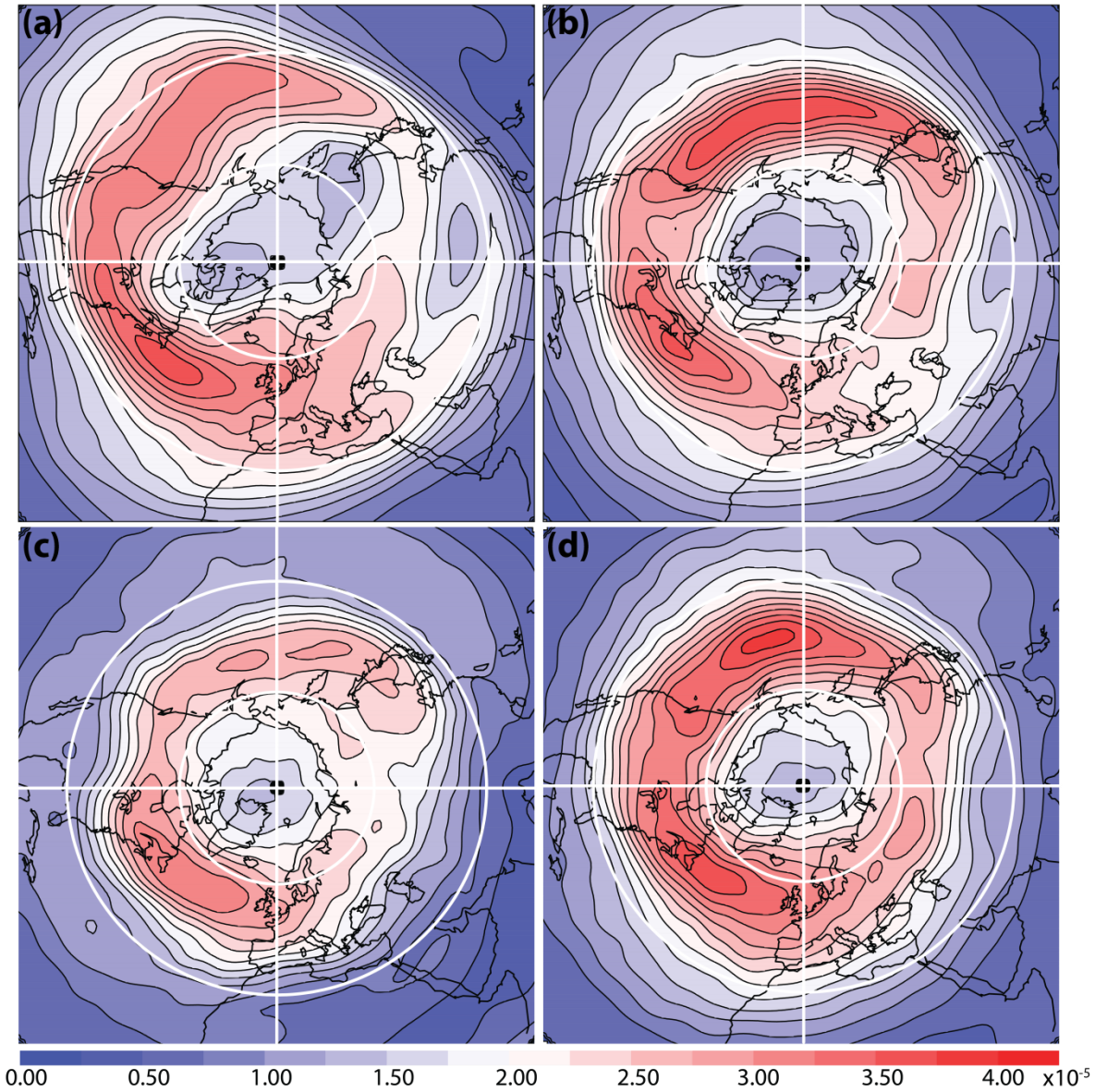

705

706 Figure 2 Standard deviation of 2-6 day band pass filtered variance of ξ_{250} for (a) DJF, (b)
707 MAM, (c) JJA and (d) SON. Units are 10^{-5} s^{-1}.

708

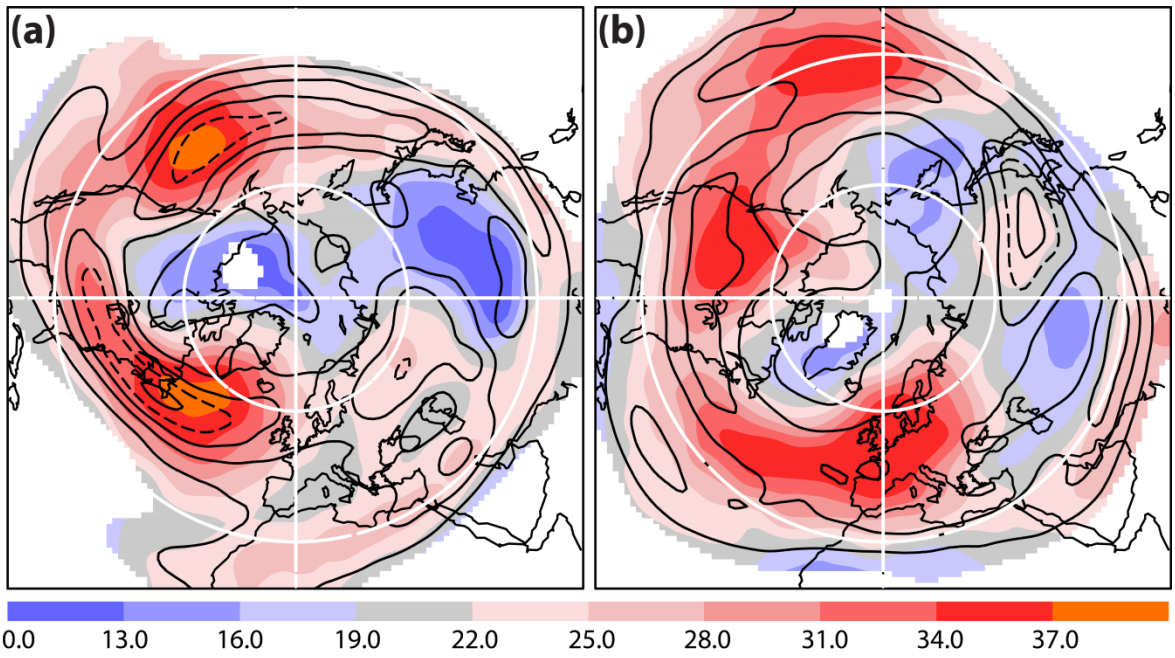

Figure 3 Track density (contours) and mean intensity (colour) for (a) positive anomalies and (b) negative anomalies in the 250hPa meridional wind (V_{250}) for DJF. Track density contours are every 2.5 with the dashed line at 10.0 in units of number per month per unit area, where the unit area is equivalent to a 5^0 spherical cap. The intensity is in units of m s^{-1}. Mean intensity is suppressed for track densities below 1.0.

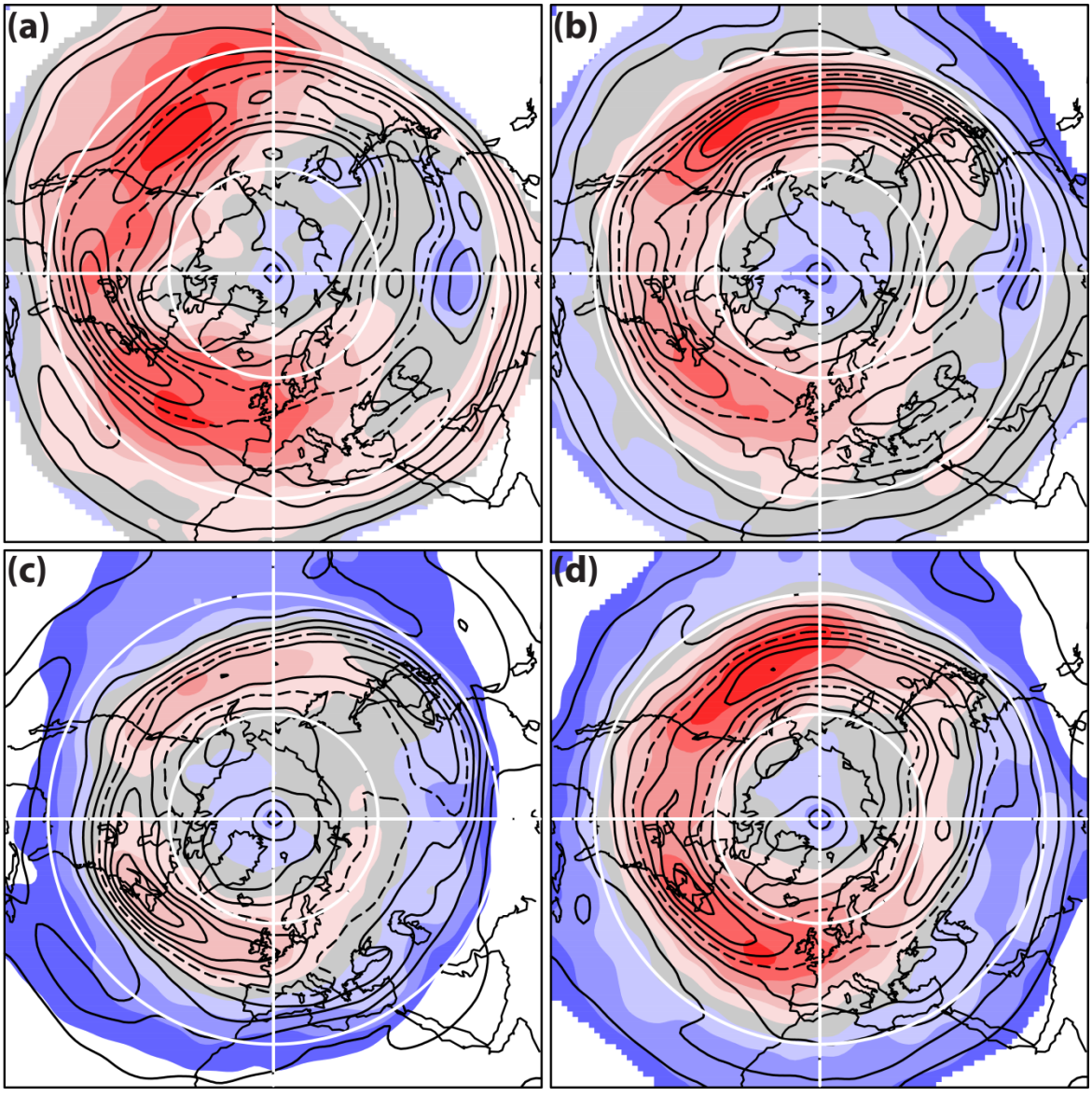

Figure 4 Track density (contours) and mean intensity (colour) for extrema in the 250hPa meridional wind (V_{250}) for each season, (a) DJF, (b) MAM, (c) JJA and (d) SON. Track density contours are every 2.5 with the dashed line at 12.5 in units of number per month per unit area, where the unit area is equivalent to a 5^0 spherical cap. The intensity is in units of m s^{-1}. Mean intensity is suppressed for track densities below 1.0.

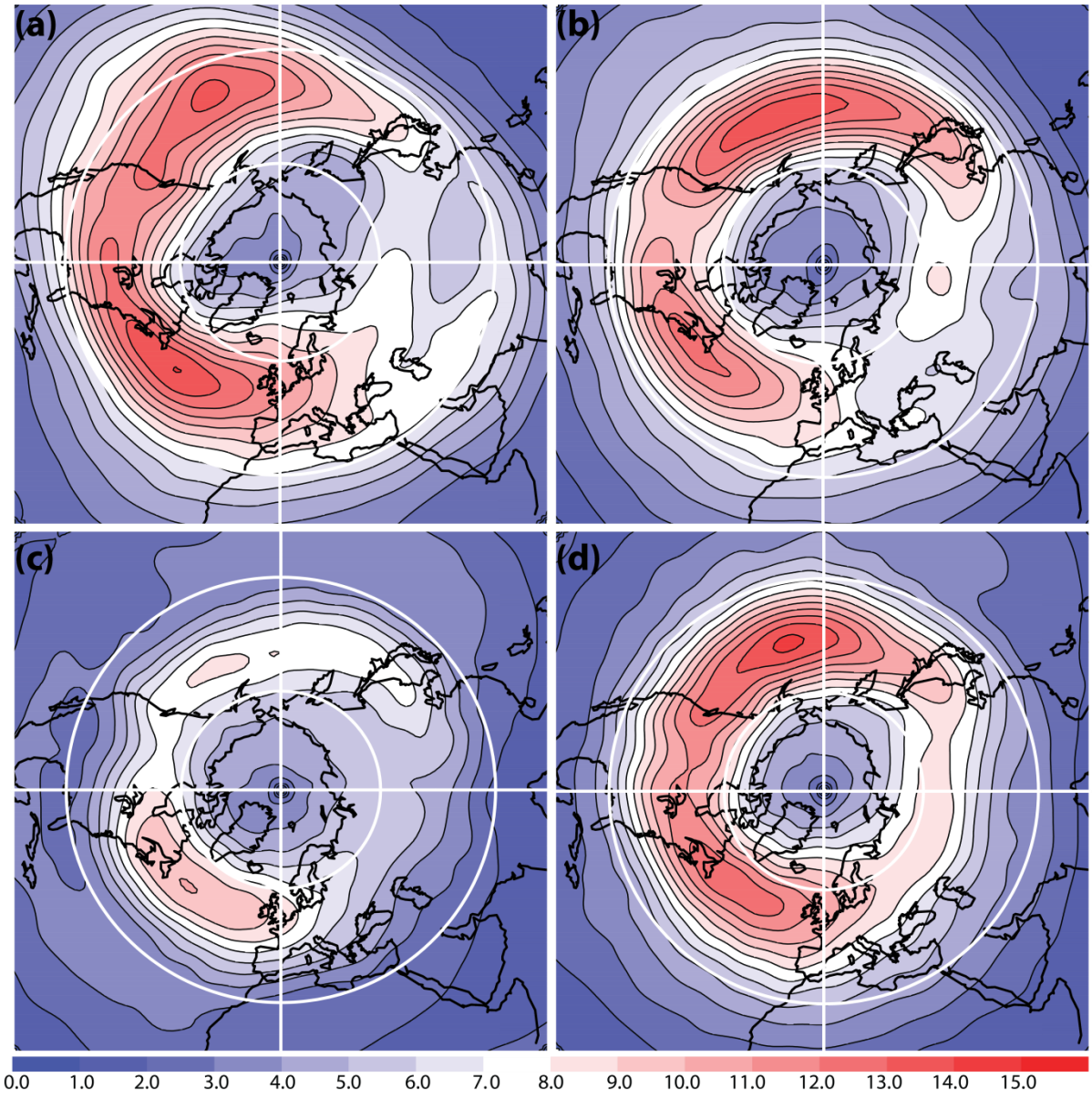

723

724 Figure 5 Standard deviation of 2-6 day band pass filtered variance of V_{250} for (a) DJF, (b)
725 MAM, (c) JJA and (d) SON. Units are m s^{-1}.

726

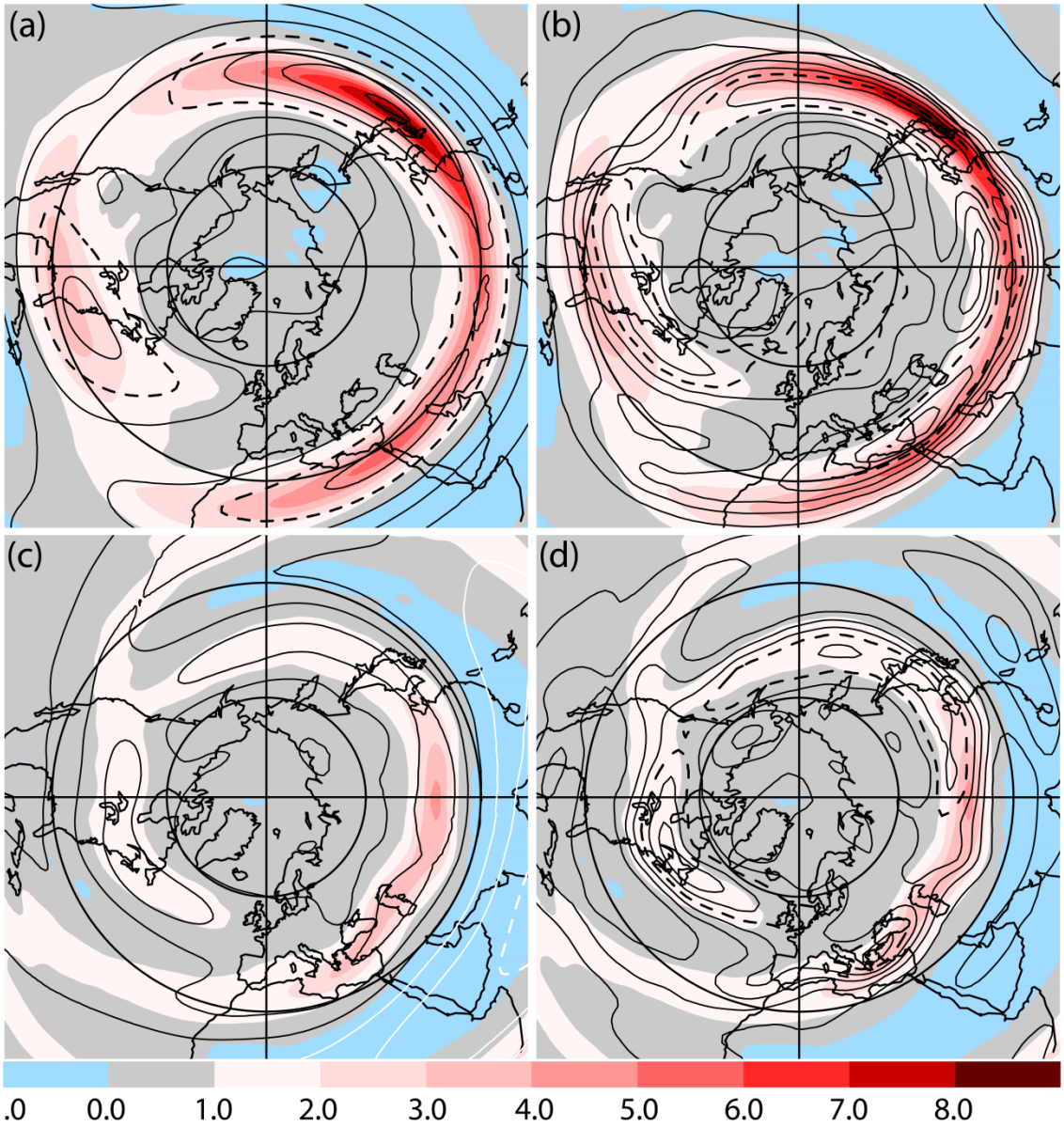

Figure 6 Tropopause level (PV=2) mean fields and the 250hPa storm-track are shown for winter (upper panels: a, b) and summer (lower panels: c, d). In each panel the mean meridional gradient of $\theta_{PV=2}$ is shown in colour with reversed sign and in units of K (100km)$^{-1}$. In the panels on the left (a, c), the overlaid field is the seasonal mean zonal wind, $U_{PV=2}$, with contours every 10ms^{-1} and negative values in white with dashed contour at ±30ms^{-1}. In the panels on the right (b, d), the overlaid field is the track density for ξ_{250} cyclones, as in Fig.1.

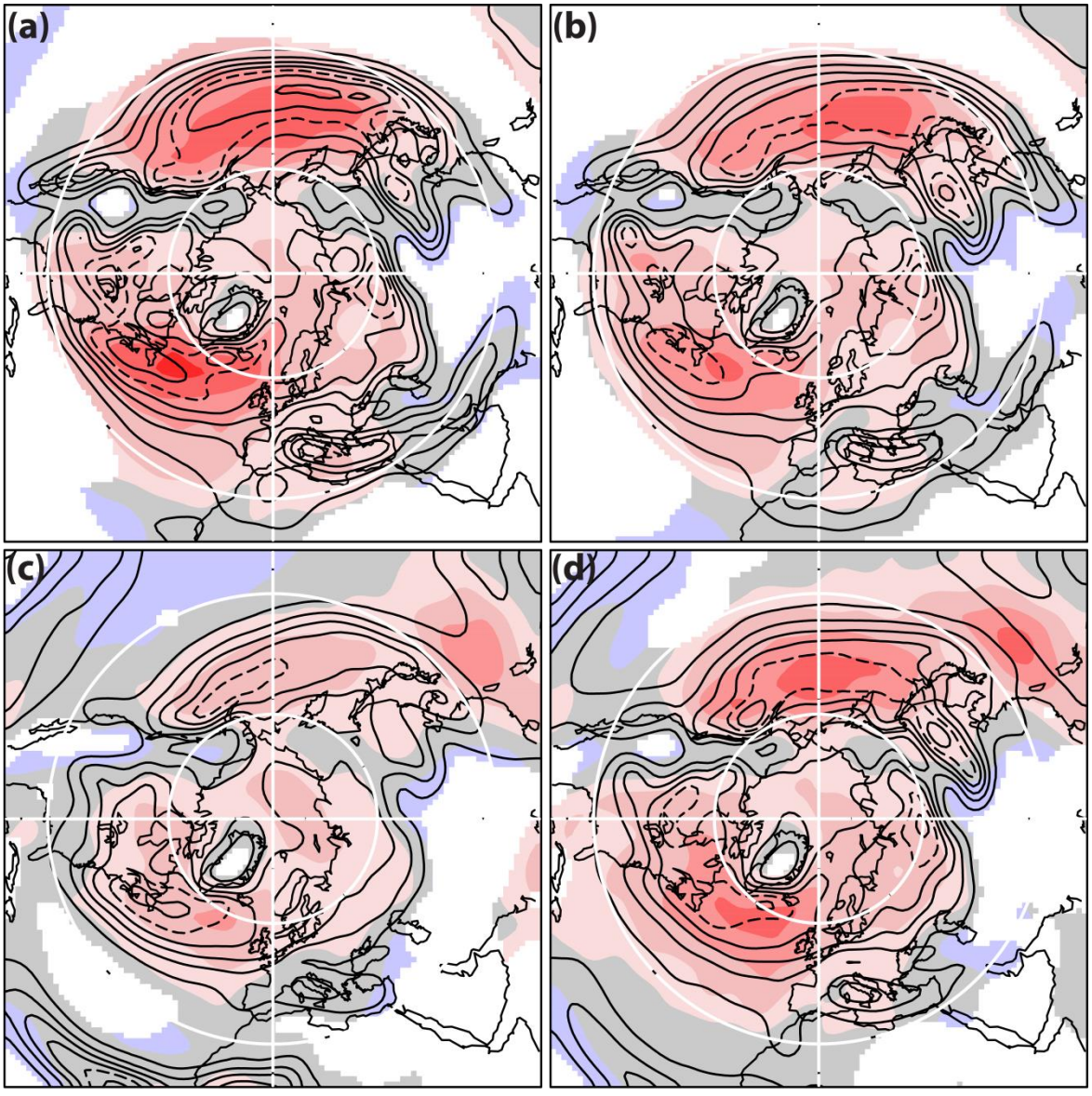

Figure 7 Track density (contours) and mean intensity (colour) of ξ_{850} cyclones for each season, (a) DJF, (b) MAM, (c) JJA and (d) SON. Track density contours are every 2.5 with the dashed line at 12.5 in units of number per month per unit area, where the unit area is equivalent to a 5^0 spherical cap. The intensity is in units of 10^{-5} s^{-1}. Mean intensity is suppressed for track densities below 1.0.

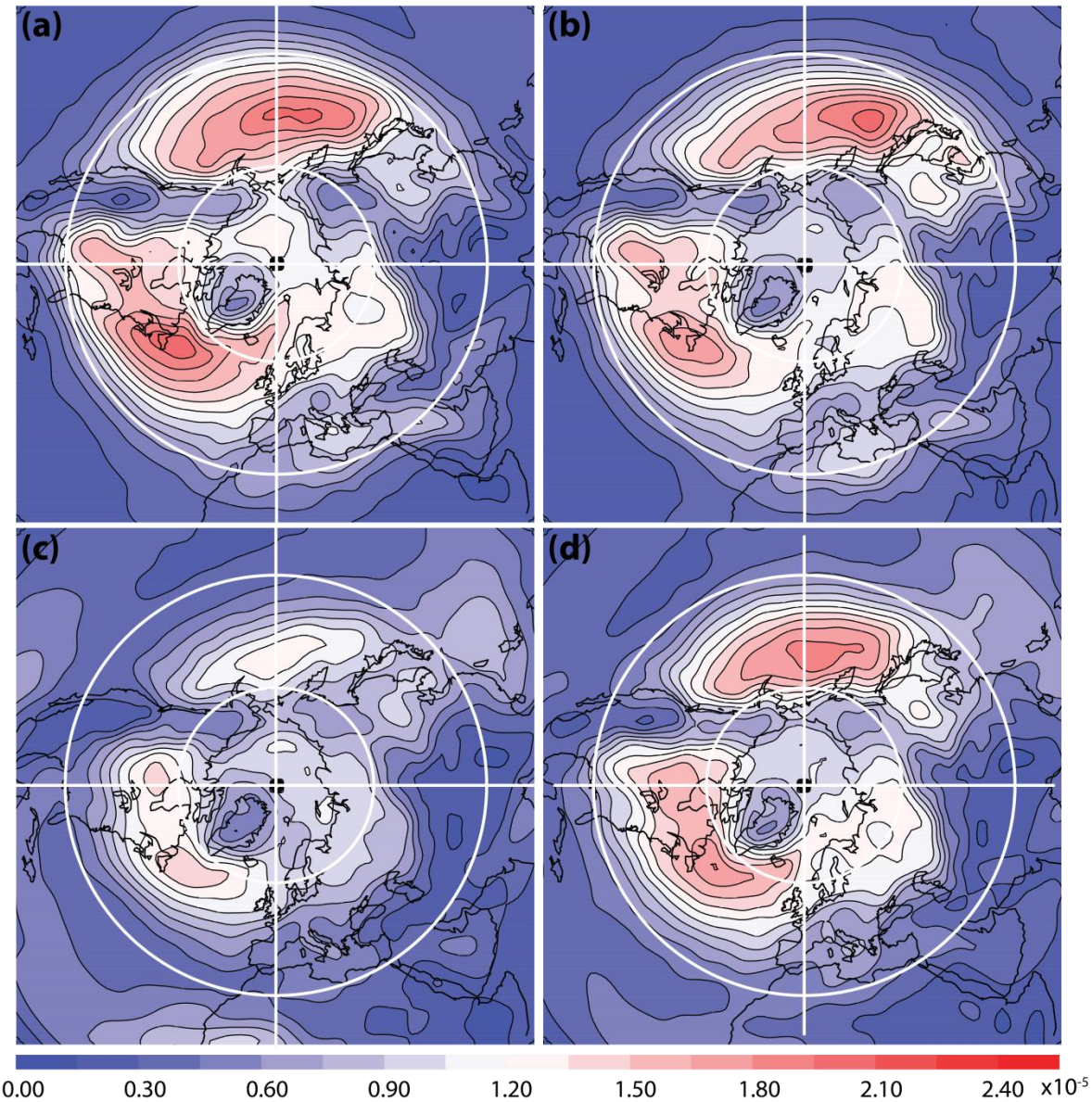

743

744 Figure 8 Standard deviation of 2-6 day band pass filtered variance of ξ_{850} for (a) DJF, (b)
745 MAM, (c) JJA and (d) SON. Units are 10^{-5} s^{-1}.

746

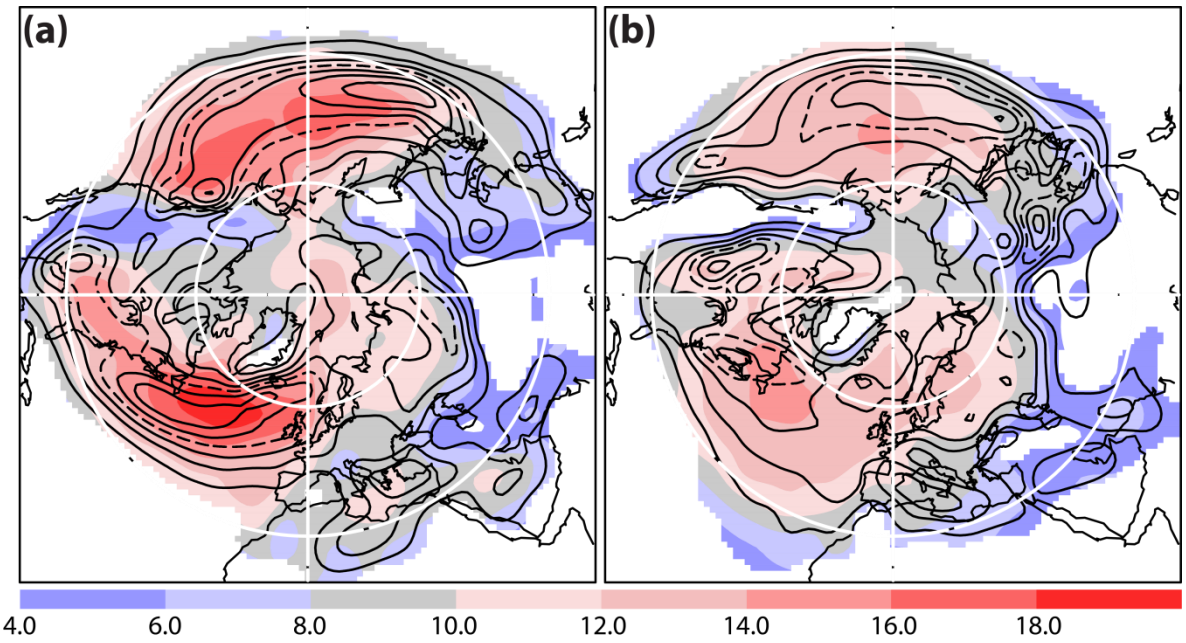

Figure 9 Track density (contours) and mean intensity (colour) for (a) positive anomalies and (b) negative anomalies in the 850hPa meridional wind (V_{850}) for DJF. Track density contours are every 2.0 with the dashed line at 8.0 in units of number per month per unit area, where the unit area is equivalent to a 5^0 spherical cap. The intensity is in units of m s^{-1}. Mean intensity is suppressed for track densities below 1.0.

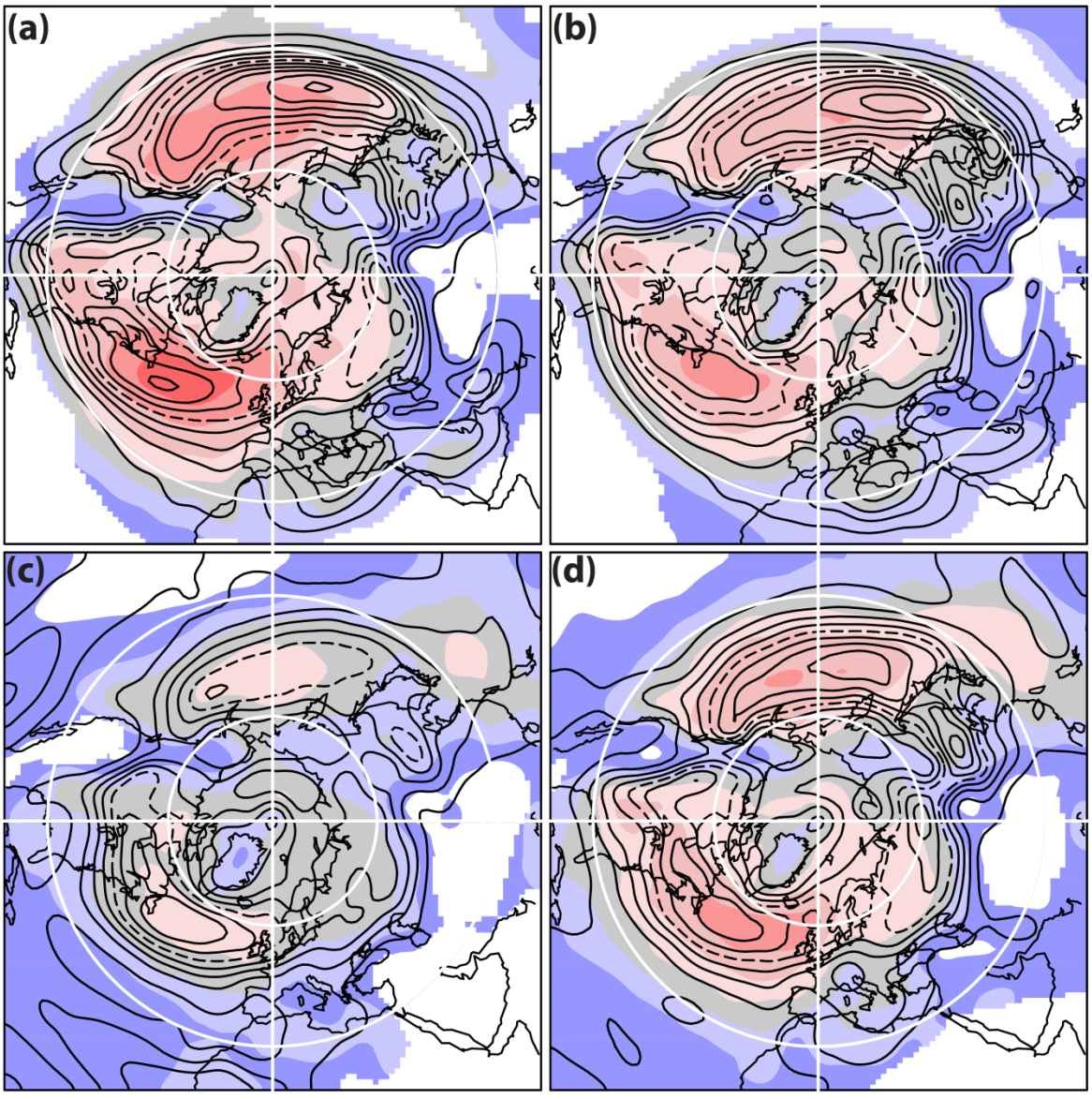

754

755 Figure 10 Track density (contours) and mean intensity (colour) for extrema in V_{850} for each
756 season, (a) DJF, (b) MAM, (c) JJA and (d) SON. Track density contours are every 2.5 with the
757 dashed line at 12.5 in units of number per month per unit area, where the unit area is
758 equivalent to a 5^0 spherical cap. The intensity is in units of m s^{-1}. Mean intensity is
759 suppressed for track densities below 1.0.

760

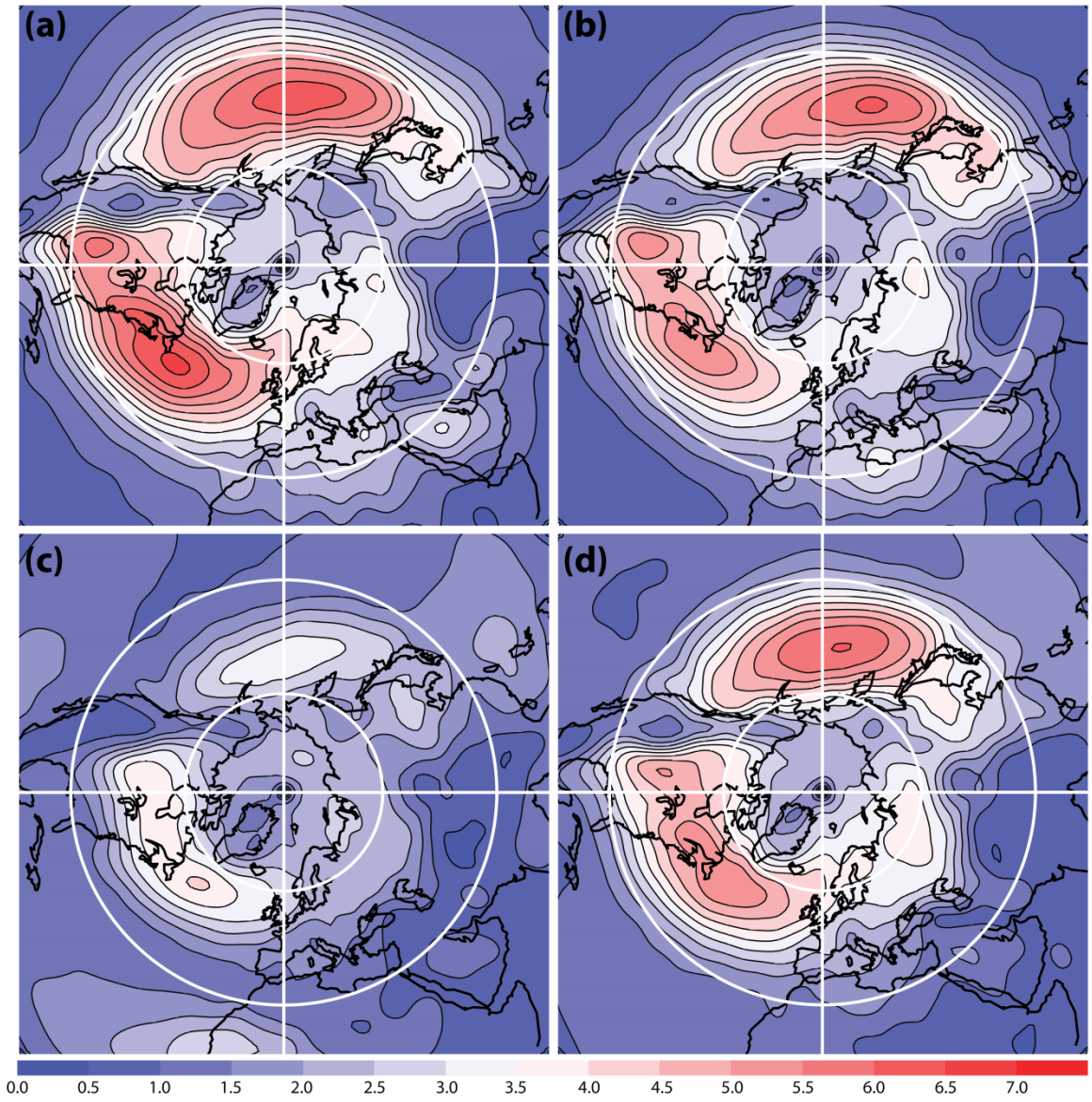

761

762 Figure 11 Standard deviation of 2-6 day band pass filtered variance of V_{850} for (a) DJF, (b)
763 MAM, (c) JJA and (d) SON. Units are m s^{-1}.

764

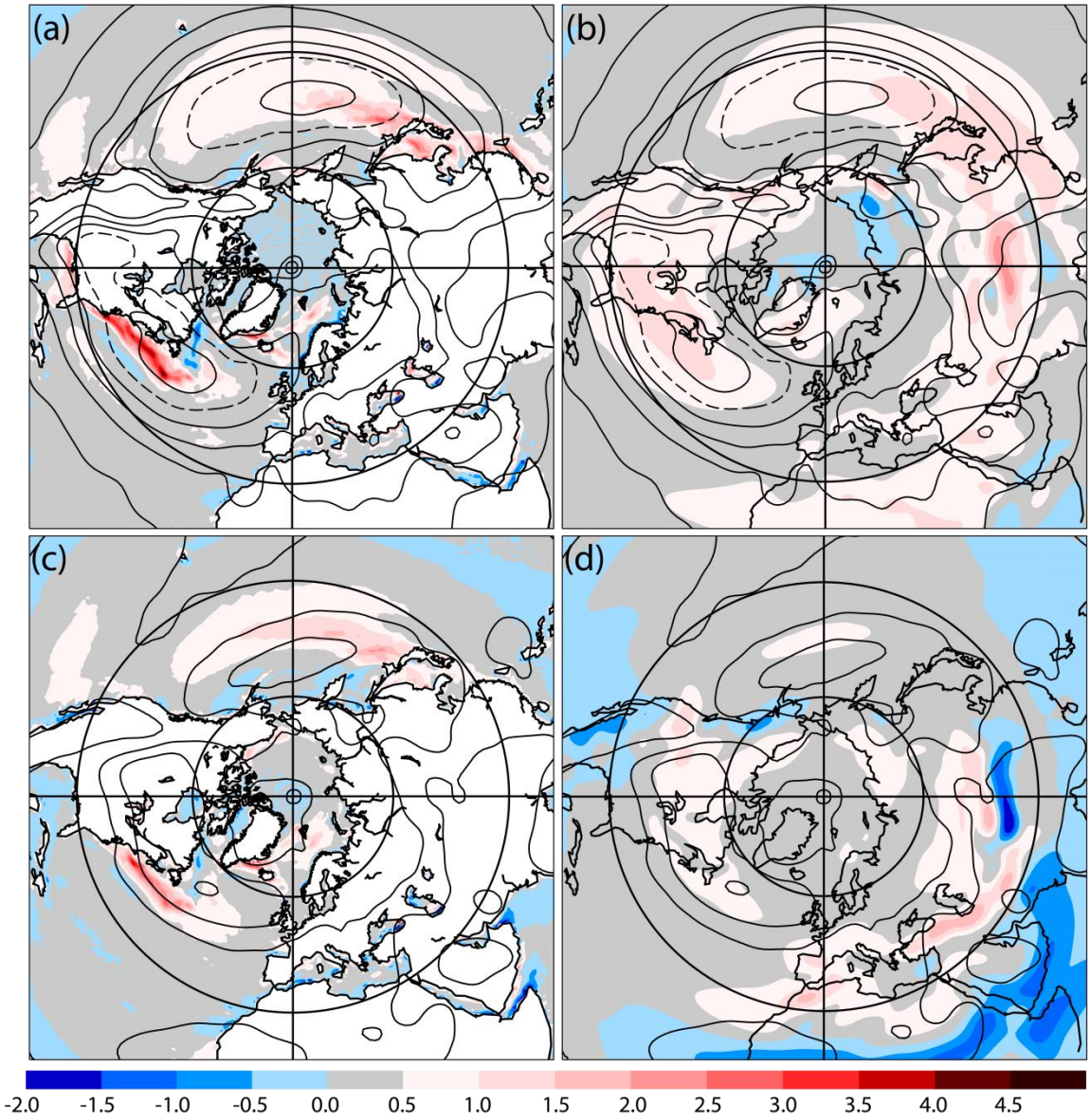

Figure 12 Low-level mean temperature gradients and the 850hPa storm-track are shown for winter (upper panels: a, b) and summer (lower panels: c, d). The contours in each panel are those of the standard deviation of 2-6 day band-pass filtered variance of V_{850} for the relevant season with contours every 1 ms^{-1} and the 5ms^{-1} contour dashed. Colour contours are for the mean meridional gradient of sea surface temperature (left: a, c) and 850hPa temperature (right: b, d). In each case, the sign has been reversed and the unit is K $(100Km)^{-1}$.